Journal of Materials Chemistry A

ROYAL SOCIETY OF CHEMISTRY

PAPER

View Article Online
View Journal | View Issue

Check for updates

Cite this: J. Mater. Chem. A, 2025, 13, 30291

Tuning the coordination microenvironment of Co sites embedded in porous organic polymer for the hydroformylation of diisobutylene

Hong Wei,†[ab] Cunyao Li,†[b] Guangjun Ji,[b] Miao Jiang,[b] Benhan Fan,[b] Sen Feng,[ab] Xinyuan Liu,[bc] Lei Ma,[b] Li Yan*[bc] and Yunjie Ding *[abd]

Hydroformylation is one of the most important routes for the synthesis of high-value-added fine chemicals, which usually relies on metal rhodium and cobalt. Diisobutylene is a chemical intermediate of great interest in the chemical industry, which could serve as a fine feedstock to prepare environmentally friendly plasticizers through the hydroformylation route. At present, the hydroformylation of diisobutylene is mainly based on homogeneous cobalt-based catalytic systems, suffering from a complicated recycling process and harsh reaction conditions. Herein, by regulating the coordination microenvironment of Co species, three Co@POPs heterogeneous catalysts, marked as Co@POPs-DVB, Co@POPs-PPh_3&DVB and Co@POPs-PPh_3, were successfully designed and synthesized. Co@POPs-PPh_3&DVB showed a superior catalytic performance with a 45.6% yield and a 78.4% selectivity for the main products (isononanal and isononanol), which was better than the homogeneous $Co(acac)_2$:PPh_3 system that offered a 29.1% yield and a 53.1% selectivity. Additionally, Co@POPs-PPh_3&DVB could maintain a high activity and selectivity for at least 5 cycles without losing activity. Various characterizations indicated that the unique structure and microenvironment of Co@POPs-PPh_3&DVB promoted the formation of $HCo(CO)_3$(P-frame) active species, which was the dominant active species for the hydroformylation of diisobutylene.

Received 23rd May 2025
Accepted 30th July 2025

DOI: 10.1039/d5ta04135j

rsc.li/materials-a

1. Introduction

Hydroformylation of olefins, which converts olefins, CO and H_2 to aldehydes and alcohols with perfect atom economy, is one of the most versatile reaction routes in the chemical industry.[1,2] Meanwhile, the high value and wide application range of aldehydes and alcohols endow the hydroformylation reaction with notable research value and application significance. Generally, Co and Rh complexes are the most common active centers in hydroformylation reactions. Rh complexes possess much higher catalytic performance and require milder reaction conditions in the hydroformylation of straight-chain olefins,[3–5] but Co[3,6–9] complexes are still the first considered catalysts for hydroformylation of complex olefins due to the decomposition of rhodium catalysts when distilling aldehyde products from the catalytic system under harsh conditions.

Among the hydroformylation of complex olefins dominated by Co-based catalysts, the hydroformylation of diisobutylene (DIB) is particularly important.[10–12] The isononanal and isononanol,[13] the main products of the DIB hydroformylation reaction, are extensively used in the chemical, food, and electronics industries. Traditionally, the hydroformylation of DIB is catalyzed by homogeneous $Co_2(CO)_8$ under rigorous reaction conditions, which also requires a series of complex processes in the separation and recycling of $Co_2(CO)_8$. Owing to their inherent advantages in separation and recovery, the development of heterogeneous Co-based catalysts for the DIB hydroformylation reaction has attracted more and more attention.[14–18] However, the poor activity and stability limit the application of heterogeneous Co-based catalysts in DIB hydroformylation.[19] Designing and synthesizing high-performance heterogeneous Co-based catalysts for the hydroformylation of DIB is still highly desired but challenging.

Due to their superior activity and stability, porous organic polymer (POP)-supported metal catalysts are used as efficient heterogeneous catalysts in many types of reactions.[20–22] Moreover, by introducing functional sites with coordination capacity, metal atoms/ions could be dispersed as single sites. This type of heterogeneous single-metal-site catalysts (SMSCs) offers maximum metal utilization[23] and has shown good catalytic performance and stability in many reactions. The emergence of single-metal-site catalysts has surely provided many

[a]Department of Chemical Physics, University of Science and Technology of China, Hefei, Anhui 230026, China
[b]Dalian National Laboratory for Clean Energy, Dalian Institute of Chemical Physics, Chinese Academy of Sciences, Dalian, Liaoning 116023, China. E-mail: yanli@dicp.ac.cn; dyj@dicp.ac.cn
[c]University of Chinese Academy of Sciences, Beijing 100049, China
[d]State Key Laboratory of Catalysis, Dalian Institute of Chemical Physics, Chinese Academy of Sciences, Dalian, Liaoning 116023, China
† These authors contributed equally to this work.

opportunities to design efficient heterogeneous hydroformylation catalysts.

POP-based SMSCs continue to attract attention and are widely applied to hydroformylation of olefins.[21,24–27] During the study,[28,29] the optimization of catalytic performance could be achieved by regulating the microenvironment of Rh–P active sites. Also, a series of single-Rh-site catalysts with Rh–P species as active sites were synthesized, and the structure–activity relationship between the catalyst structure and its catalytic performance in straight-chain olefins was carefully studied in our previous works.[23,30,31] In addition to Rh, some other metal single-atom catalysts, such as Ru-based catalysts,[32] Au-based catalysts[33] and Co-based catalysts,[19] have also been successfully applied to the hydroformylation reaction. Inspired by these studies, single-Co-site catalysts (denoted as Co@POPs) were successfully designed and synthesized for the hydroformylation of complex olefins. By regulating the pore structure of polymers, the ratio of $HCo(CO)_3$(P-frame) and $HCo(CO)_2$(P-frame)$_2$ species was altered during the hydroformylation of DIB. Consequently, Co@POPs-PPh_3&DVB showed superior catalytic performance with a 45.6% yield and a 78.4% selectivity to the main products (isononanal and isononanol), which is even better than the homogeneous $Co(acac)_2$:PPh_3 system with a 29.1% yield and a 53.1% selectivity. Multiple characterization methods were employed to confirm the effectiveness of our approach.

2. Experimental section

2.1 Materials

All solvents were purified according to standard laboratory methods. 4-Bromostyrene (98%) and PCl_3 (97%) were purchased from Aladdin. Tetrahydrofuran (THF, 98%), azodiisobutyronitrile (AIBN, 98%), acetylacetone cobalt ($Co(acac)_2$, 97%), divinylbenzene (DVB, 80%), diisobutylene (DIB, 98%) and toluene (99%) were purchased from Shanghai Macklin Biochemical Technology Co., Ltd. THF was distilled over sodium/benzophenone under an Ar atmosphere.

2.2 Synthesis procedure

All operations were performed in the glove box or using the standard Schlenk technique. The synthesis processes were reported in the previous literature.[25,34]

Synthesis of 3v-PPh_3: 40 ml THF solution of 4-bromostyrene (60 mmol) was added dropwise to magnesium chips (63 mmol) over 1 h to avoid excessive heat release. After the addition was complete, the mixture was stirred for 4 h until magnesium dissolution. 20 mmol of PCl_3 was dissolved in a small amount of THF, introduced dropwise to the above solution at −20 °C. After two hours of the reaction, the reaction was quenched with 50 ml of saturated NH_4Cl(aq). The organic phase was extracted with ethyl acetate (3 × 30 ml) and dried over anhydrous $MgSO_4$. After the residue was purified by silica gel column chromatography, a white solid (3v-PPh_3) was obtained.

Synthesis of Co@POPs-DVB: the catalyst was prepared using a solvothermal copolymerization method. In a typical process, 0.25 g (1 mmol) of $Co(acac)_2$ was added to a 50 ml reaction kettle containing 40 ml THF solution and stirred for 10 minutes to form a uniform solution. Then, 1.7 g of DVB (13 mmol) was added and stirred at room temperature for 24 hours. Next, 0.064 g of AIBN was added, and the gelatinous solid was obtained by keeping the kettle in an oven at 110 °C for 24 hours. After drying at 25 °C under vacuum for 6–8 hours, the Co@POPs-DVB was obtained.

Synthesis of Co@POPs-PPh_3&DVB: The catalyst was prepared by a solvothermal copolymerization method. In a typical process, 0.25 g (1 mmol) of $Co(acac)_2$ was added to a 50 ml reaction kettle containing 40 ml THF solution and stirred for 10 minutes to form a uniform solution. Then, 0.68 g (2 mmol) of 3v-PPh_3 was added and stirred at room temperature for 24 hours. Next, 1.02 g of DVB and 0.064 g of AIBN were added, and the gelatinous solid was obtained by keeping the kettle in an oven at 110 °C for 24 hours. After drying at 25 °C under vacuum for 6–8 hours, Co@POPs-PPh_3&DVB was obtained. Notably, Co@POPs-PPh_3&DVB in this study refers to the molar ratio of 3v-PPh_3 to DVB, which is 3 : 10.

Synthesis of Co@POPs-PPh_3: the catalyst was prepared by a solvothermal copolymerization method. In a typical process, 0.25 g (1 mmol) of $Co(acac)_2$ was added to a 50 ml reaction kettle containing 40 ml THF solution and stirred for 10 minutes to form a uniform solution. Then, 1.7 g (5 mmol) of 3v-PPh_3 was added and stirred at room temperature for 24 hours. Next, 0.064 g of AIBN was added, and the gelatinous solid was obtained by keeping the kettle in an oven at 110 °C for 24 hours. After drying at 25 °C under vacuum for 6–8 hours, Co@POPs-PPh_3 was obtained.

2.3 Catalytic performance evaluation

Hydroformylation procedure: the hydroformylation of diisobutylene (DIB) was conducted in a 50 ml stainless steel autoclave with temperature control and mechanical stirring. A typical reaction mixture contained 0.06 g of the Co@POPs-DVB catalyst (either Co@POPs-PPh_3&DVB or Co@POPs-PPh_3), 0.6 g of DIB, and 6 g of toluene. After sealing, the reactor was purged three times with syngas (CO/H_2) and pressurized to 4.0 MPa. The mixture was heated to 155 °C over 30 min and maintained for 4 h. The reaction was quenched by ice-water cooling, followed by pressure release. Products were analyzed using an Agilent 8890 GC with a DB-FFAP column (30 m × 320 μm × 0.25 μm) and FID detector.

For catalyst recycling, the used catalyst was recovered by centrifugation under an inert atmosphere and directly reused.

Homogeneous system comparison: the control experiments employed cobalt precursors under identical conditions: 0.0327 mmol $Co(acac)_2$, 0.0164 mmol $Co_2(CO)_8$, or 0.0327 mmol $Co(acac)_2$ with 0.0654 mmol PPh_3.

3. Results and discussion

To confirm the formation of the polymer backbone, Co@POPs-PPh_3&DVB and Co@POPs-PPh_3 were selected as representative samples and characterized by ^{13}C MAS NMR. As shown in Fig. 1(a), the signal ranging from 19 to 57 ppm was attributed to

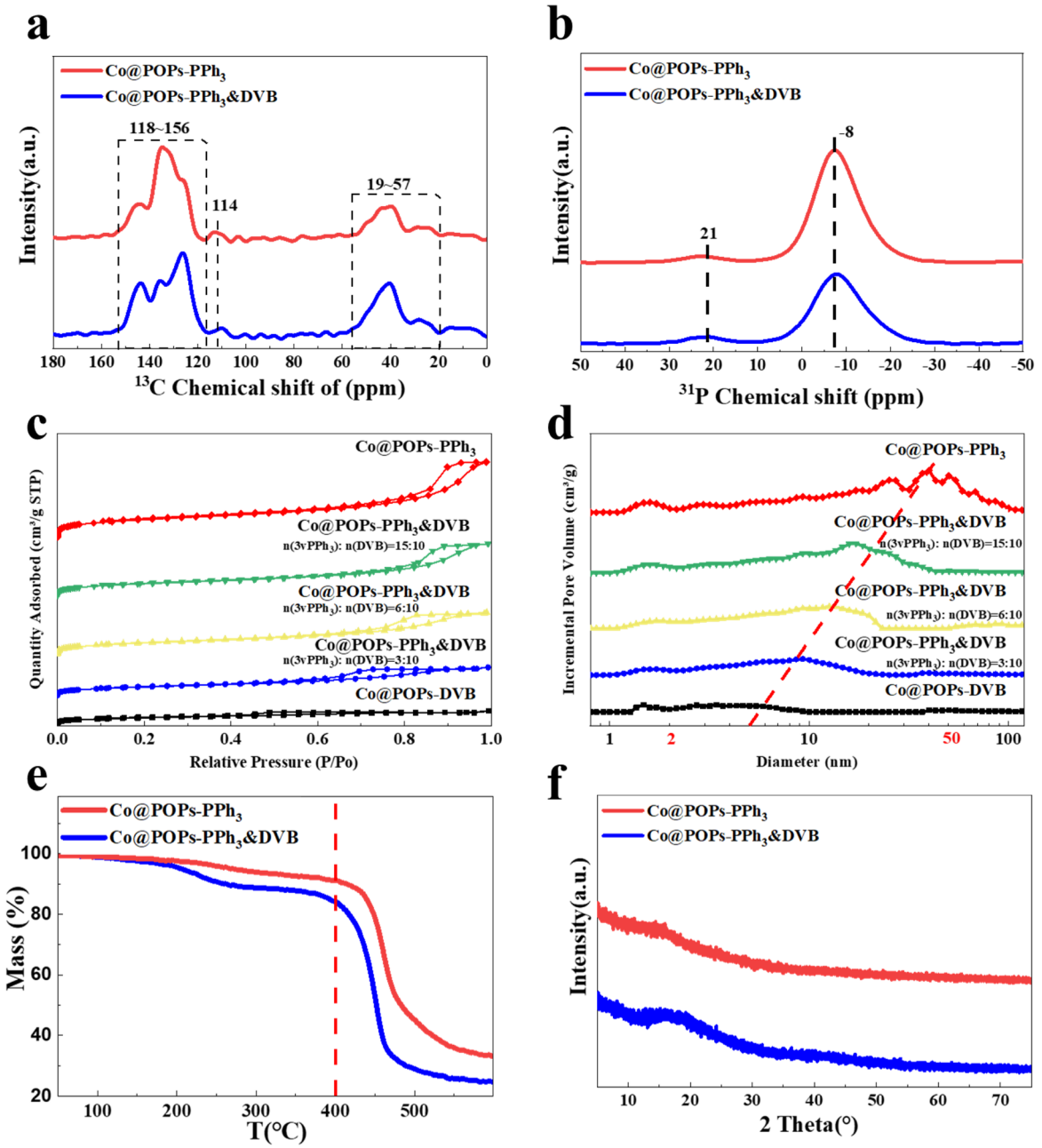

Fig. 1 (a) ^{13}C MAS NMR spectra of Co@POPs-PPh$_3$&DVB and Co@POPs-PPh$_3$; (b) ^{31}P MAS NMR spectra of Co@POPs-PPh$_3$&DVB and Co@POPs-PPh$_3$; (c) nitrogen physical adsorption curves of Co@POPs-DVB and Co@POPs-PPh$_3$&DVB note: n(3vPPh$_3$) : n(DVB) = 3 : 10 represents that the molar ratio of 3v-PPh$_3$ and DVB is 3 : 10, Co@POPs-PPh$_3$&DVB. Note: n(3vPPh$_3$) : n(DVB) = 6 : 10 represents that the molar ratio of 3v-PPh$_3$ and DVB is 6 : 10, Co@POPs-PPh$_3$&DVB. Note: n(3vPPh$_3$) : n(DVB) = 15 : 10 represents that the molar ratio of 3v-PPh$_3$ and DVB is 15 : 10, and Co@POPs-PPh$_3$; (d) pore distribution curves of Co@POPs-DVB and Co@POPs-PPh$_3$&DVB note: n(3vPPh$_3$) : n(DVB) = 3 : 10 represents that the molar ratio of 3v-PPh$_3$ and DVB is 3 : 10, Co@POPs-PPh$_3$&DVB. Note: n(3vPPh$_3$) : n(DVB) = 6 : 10 represents that the molar ratio of 3v-PPh$_3$ and DVB is 6 : 10, Co@POPs-PPh$_3$&DVB. Note: n(3vPPh$_3$) : n(DVB) = 15 : 10 represents that the molar ratio of 3v-PPh$_3$ and DVB is 15 : 10, and Co@POPs-PPh$_3$; (e) TG curves of Co@POPs-PPh$_3$&DVB and Co@POPs-PPh$_3$; and (f) XRD patterns of Co@POPs-PPh$_3$&DVB and Co@POPs-PPh$_3$. Note: in the Co@POPs-PPh$_3$&DVB sample, the molar ratio of 3v-PPh$_3$ to DVB is 3 : 10.

the polymerized vinyl groups of Co@POPs-PPh$_3$&DVB,[21,29,31,35] while the strong signal ranging from 118 to 156 ppm was due to the chemical shift of aromatic carbons of Co@POPs-PPh$_3$&DVB. The weak signal peak at 114 ppm belongs to the unpolymerized vinyl groups,[29,36] which was much weaker than that of polymerized vinyl groups, indicating that most vinyl groups participate in the free-radical polymerization to form the polymer framework. Similarly, ^{13}C MAS NMR of Co@POPs-PPh$_3$ also showed that it was highly polymerized. However, the signal of the polyethylene group in Co@POPs-PPh$_3$&DVB was significantly stronger than that in Co@POPs-PPh$_3$, which originated from the higher vinyl density of the comonomer (DVB) in

Co@POPs-PPh_3&DVB. The stronger polyethylene group signal indicated that DVB successfully copolymerizes with 3v-PPh_3, which might increase the rigidity of the polymer. As for the ^{31}P MAS NMR spectra of Co@POPs-PPh_3&DVB and Co@POPs-PPh_3 (Fig. 1(b)), there were two signal peaks. The main signal at −8 ppm was attributed to P atoms in the polymer backbone.[24,31] The weak signals at 21 ppm were attributed to slightly oxidized phosphine (P═O) and phosphine coordinated with Co, respectively. Obviously, the signal peak of the P atom of Co@POPs-PPh_3&DVB was slightly weaker than that of Co@POPs-PPh_3, further indicating that DVB was indeed introduced into the polymer backbone.

In order to clarify the pore characteristics of Co@POPs, nitrogen physical adsorption was employed. Fig. 1(c) shows that all catalysts exhibit the curve of type I plus type-IV,[37] indicating the inherent hierarchical porosities of catalysts. The pore size distribution curves (Fig. 1(d)) of Co@POPs-DVB, Co@POPs-PPh_3&DVB (n(3vPPh$_3$) : n(DVB) = 3 : 10), Co@POPs-PPh_3&DVB (n(3vPPh$_3$) : n(DVB) = 6 : 10), Co@POPs-PPh_3&DVB (n(3vPPh$_3$) : n(DVB) = 15 : 10), and Co@POPs-PPh_3, ranging from 1 to 100 nm, were calculated using density functional theory (DFT). As shown in Table S1, Co@POPs-PPh_3 possessed the highest BET surface area, the largest pore volume and the largest adsorption-average pore diameter, which are 851 $m^2\ g^{-1}$, 2.31 $cm^3\ g^{-1}$ and 10.85 nm, respectively. Interestingly, these parameters exhibited a regular decrease with an increase in the amount of DVB. The BET surface area, pore volume and adsorption-average pore diameter of Co@POPs-DVB were the lowest in all catalysts. These results imply that DVB with a small volume and high vinyl density participates in the formation of the polymer backbone and effectively improves the crosslinking degree and rigidity of polymers. Moreover, the average pore size, which was approximately 40 nm in Co@POPs-PPh_3, dropped to around 5 nm in Co@POPs-DVB. This distinct alteration might significantly influence the equilibrium of active species and the distribution of products.

The morphological features of Co@POPs-PPh_3&DVB and Co@POPs-PPh_3 were detected by SEM and TEM. As shown in Fig. 2(a) and (g), Co@POPs-PPh_3&DVB and Co@POPs-PPh_3 consisted of plentiful aggregated irregular particles and exhibited hierarchical porosities. The porous structure was conducive to the dispersion of metals and the diffusion of substrates and products. The corresponding EDS mapping (Fig. 2(d)–(f) and (j)–(l)) of Co@POPs-PPh_3&DVB and Co@POPs-PPh_3 demonstrated the uniform dispersion of functional elements (C, P, Co). As shown in Fig. 4(a), no Co–Co bond was observed on Co@POPs-PPh_3&DVB and Co@POPs-PPh_3 by EXAFS, indicating that cobalt was distributed in the form of single sites on the polymers. Fig. 4(d) further confirms that Co is in a single-atom form in Co@POPs-PPh_3&DVB.

To disclose the interactions between Co and P, XPS characterization analysis was employed. Fig. 3(a) displays the Co 2p XPS binding energy of Co@POPs-PPh_3&DVB and Co@POPs-PPh_3, where two shoulder peaks appear due to multielectron excitations.[38,39] Taking [Co(acac)$_2$] as reference, the peaks of Co $2p_{3/2}$ and Co $2p_{1/2}$ appear at 781.1 and 796.7 eV, which are downshifted to 780.9 and 796.5 eV for Co@POPs-PPh_3&DVB and 780.7 and 796.3 eV for Co@POPs-PPh_3, respectively. This

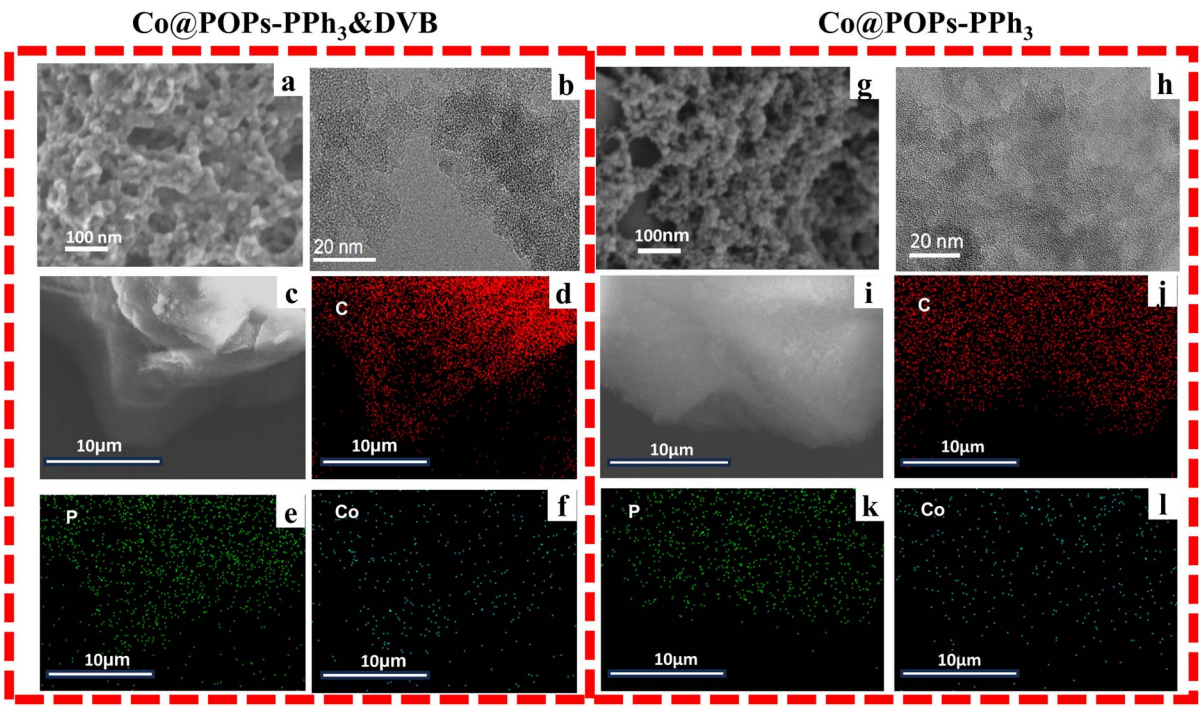

Fig. 2 (a) SEM image of Co@POPs-PPh_3&DVB; (b) TEM image of Co@POPs-PPh_3&DVB; (c–f) SEM image and corresponding EDS elemental mappings of Co@POPs-PPh_3&DVB; (g) SEM image of Co@POPs-PPh_3; (h) TEM image of Co@POPs-PPh_3; and (i–l) SEM image and corresponding EDS elemental mappings of Co@POPs-PPh_3. Note: in the Co@POPs-PPh_3&DVB sample, the molar ratio of 3v-PPh_3 to DVB is 3 : 10.

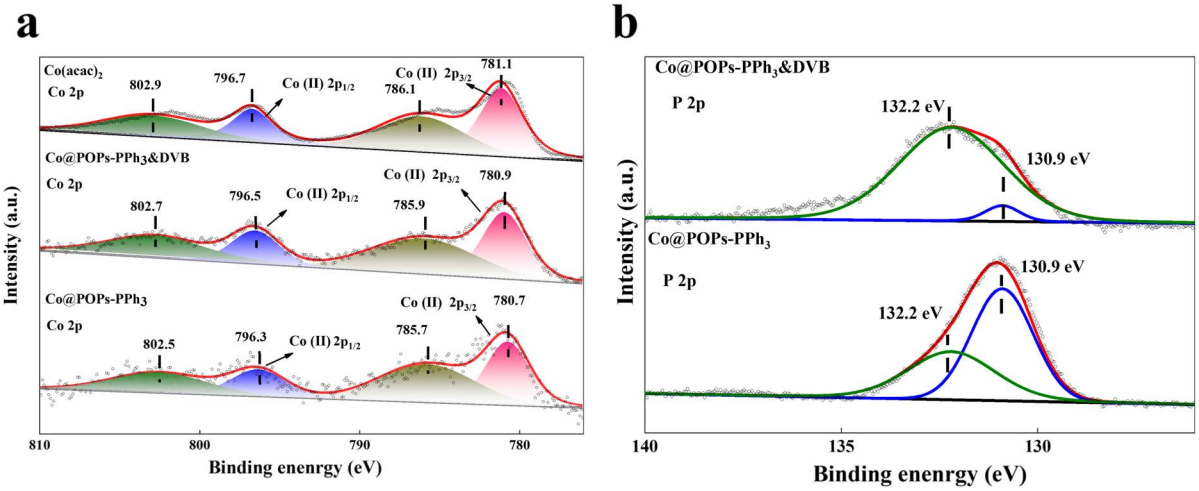

Fig. 3 (a) Co 2p and (b) P 2p XPS spectra of Co@POPs-PPh_3&DVB and Co@POPs-PPh_3. Note: in the Co@POPs-PPh_3&DVB sample, the molar ratio of 3v-PPh_3 to DVB is 3 : 10.

phenomenon is based on the fact that the lone electrons of P in the polymer fill the empty orbital of Co, and the density of the outer electron cloud of Co increases, resulting in a decrease in the constraint of the nucleus on the p orbital electrons. In other words, the reduction in the Co 2p binding energy is due to the coordination interaction between Co and P. In Fig. 3(b), the P 2p binding energy of Co@POPs-PPh_3&DVB and Co@POPs-PPh_3 showed obvious differences. For Co@POPs-PPh_3&DVB, the P 2p binding energy of the coordinated P with Co ion is the main signal (the peak at 132.2 eV), and the P 2p binding energy of the P atom is a weak signal (the peak at 130.9 eV). It indicated that most of the P atoms are involved in coordination with Co ions. As for Co@POPs-PPh_3, a main peak at 130.9 eV was ascribed to the uncoordinated P 2p binding energy,[40] and the P 2p binding energy of P coordinated to Co ions was 132.2 eV. Comparing the intensities of the two peaks revealed that only a part of P participated in the coordination with the Co ion, and many uncoordinated P remained in the support. Notably, the Co 2p binding energy of Co@POPs-PPh_3&DVB was higher than that of Co@POPs-PPh_3, indicating that Co in the former was in a microenvironment with a lower P coordination number.

EXAFS was further employed to unveil the coordination environment of Co@POPs-PPh_3&DVB and Co@POPs-PPh_3. The EXAFS fitting for Co@POPs-PPh_3&DVB and Co@POPs-PPh_3 is shown in Fig. 4(b) and (c). EXAFS spectra of Co@POPs-PPh_3&DVB were fitted satisfactorily with a Co–O scattering path (R = 1.88 Å), and a Co–P scattering path (2.32 Å). Fitting of the EXAFS spectra indicated that Co was coordinated to 2.1 O atoms and 1.9 P atoms (Table S1) in the first coordination shell, providing additional evidence of the interaction of Co with P. On the other hand, the Co@POPs-PPh_3 EXAFS data were satisfactorily fitted with a Co coordination model including 2.0 O atoms and 2.0 P atoms (Table S1). As shown in Fig. 4(d), EXAFS fitting results proved the activation process of the mononuclear species Co(acac)(P-frame)$_2$. Compared with Co@POPs-PPh_3, there are fewer P atoms (including coordinated and free P atoms) around Co on Co@POPs-PPh_3&DVB.

In situ DRIFTS was performed to characterize the active species of Co@POPs-PPh_3&DVB and Co@POPs-PPh_3. The infrared spectra of Co@POPs-PPh_3&DVB and Co@POPs-PPh_3 showed that the CO vibration peaks could be unequivocally attributed to the interaction between CO and Co. In Fig. 5(a) and (b), the evolution of CO was tracked. With the introduction of syngas, the CO adsorption signal from 1944 cm^{-1} to 2170 cm^{-1} gradually increased. After the syngas was withdrawn and N_2 was purged, gaseous CO disappeared[19] (the peaks at 2170 and 2115 cm^{-1}) and the vibration peaks of linear adsorption of CO gradually weakened, indicating that Co was sensitive to the CO partial pressure. Fig. 5(c) shows the specific location of the CO adsorption peaks. In Co@POPs-PPh_3&DVB, five absorption peaks were observed; the peaks at 2074, 2050 and 1980 cm^{-1} were attributed to $HCo(CO)_3$(P-frame), and the peaks at 2028 and 2000 cm^{-1} were attributed to $HCo(CO)_2$(P-frame)$_2$. For Co@POPs-PPh_3, five adsorption peaks could be observed; peaks at 2050, 2033, and 1944 cm^{-1} were attributed to $HCo(CO)_3$(P-frame) and 2000 and 1978 cm^{-1} were attributed to $HCo(CO)_2$(P-frame)$_2$.[41–44] Compared with the Co@POPs-PPh_3 spectrum, the proportion of active species $HCo(CO)_3$(P-frame) in Co@POPs-PPh_3&DVB was higher. Furthermore, the absorption peak intensity of Co@POPs-PPh_3&DVB was much stronger than that of Co@POPs-PPh_3. In other words, both Co@POPs-PPh_3&DVB and Co@POPs-PPh_3 can form $HCo(CO)_3$(P-frame) and $HCo(CO)_2$(P-frame)$_2$; however, the proportion of $HCo(CO)_3$(P-frame) in Co@POPs-PPh_3&DVB was higher than that of Co@POPs-PPh_3 in the same syngas atmosphere. The cobalt center of $HCo(CO)_3$(P-frame) was occupied by a P atom confined in the polymer framework, which optimized the electron cloud density of the cobalt center and minimized the crowding around Co. This configuration was conducive to the adsorption and activation of substrates with large steric hindrance. On the contrary, $HCo(CO)_2$(P-frame)$_2$ was occupied by two P atoms, the electrophilicity of Co was weakened, and the Co center was more crowded, which was not conducive to the adsorption and activation of substrates.

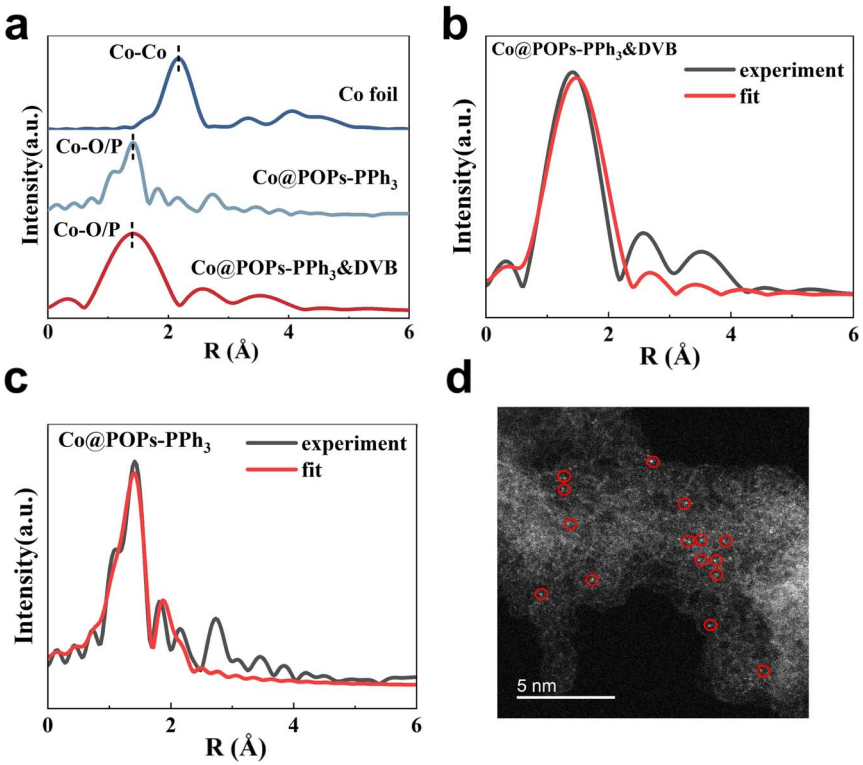

Fig. 4 (a) k^2-weighted Fourier transform spectra from Co K-edge EXAFS of Co foil, Co@POPs-PPh_3&DVB and Co@POPs-PPh_3; (b) and (c) fitting results of EXAFS spectra of Co@POPs-PPh_3&DVB and Co@POPs-PPh_3; and (d) atomic-resolution HAADF-STEM image of Co@POPs-PPh_3&DVB.

As illustrated in Fig. 6(b), the catalytic performance of cobalt complexes and Co@POPs in the hydroformylation of diisobutylene (DIB) was evaluated. Among the homogeneous cobalt complexes tested, $Co(acac)_2$ achieves the highest yield and selectivity of oxygenates, which were 62.5% and 76.8% respectively. However, the addition of PPh_3 resulted in a decrease in both the yield and selectivity of oxygenated compounds, with values dropping to 29.1% and 53.1%, respectively. The catalytic behavior of Co@POPs differed from that of the homogeneous cobalt complexes. For instance, Co@POPs-DVB showed a yield of 63.8% and selectivity of 77.7% for oxygenated compounds. When P atoms were introduced into the polymer matrix (Co@POPs-PPh_3&DVB), the yield of oxygenated compounds decreased to 45.6%, while the selectivity for oxygen-containing compounds increased slightly to 78.4%. However, with a further increase in the amount of P atoms in the polymer (Co@POPs-PPh_3), the yield of oxygenated compounds remained relatively stable at 29.7% while the selectivity for oxygen-containing compounds decreased to 42.7%.

Stability is a crucial factor in assessing the performance of heterogeneous catalysts. As illustrated in Fig. 6(c), Co@POPs-DVB, which did not have P atom doping, displayed significant deactivation after one use. In contrast, both Co@POPs-PPh_3&DVB and Co@POPs-PPh_3 demonstrated the ability to be reused 5 times without significant deactivation, indicating P atoms could substantially enhance catalyst stability. It is important to note that while the introduction of P atoms improved stability, an excessive amount could reduce the yield and selectivity of oxygenated compounds. In summary, Co@POPs-PPh_3&DVB exhibited the optimal catalytic performance, characterized by high hydroformylation activity, selectivity and stability.

The enhanced catalytic performance of Co@POPs-PPh_3&DVB in alkene hydroformylation stemmed from its carefully designed structure and the preferential activation of a sterically favored catalytic cycle. Upon exposure to syngas (CO/H_2), the precursor $HCo(acac)(P\text{-frame})_2$ undergoes ligand substitution, eliminating the acetylacetonate group to form two distinct active species (Scheme 1): $HCo(CO)_3$(P-frame) and $HCo(CO)_2(P\text{-frame})_2$. Crucially, the porous organic framework of Co@POPs-PPh_3&DVB, featuring improved polymer rigidity and reduced pore size, promotes the formation of $HCo(CO)_3$(P-frame).

Comparative analysis of cycle 1 and cycle 2 reveals detailed differences between $HCo(CO)_3$(P-frame) and $HCo(CO)_2(P\text{-frame})_2$. In cycle 1, $HCo(CO)_3$(P-frame) may promote rapid CO dissociation to provide unsaturated adsorption sites, ensuring efficient diisobutylene adsorption. In cycle 2, $HCo(CO)_2(P\text{-frame})_2$ coordinates with two P atoms and the electron cloud density of Co increases, which increases the strength of the Co–CO bond and is not conducive to the rapid dissociation of CO. In addition, the steric hindrance of $HCo(CO)_2(P\text{-frame})_2$ is greater than that of $HCo(CO)_3$(P-frame), which is not conducive to diisobutylene adsorption. Therefore, $HCo(CO)_3$(P-frame) exhibited higher hydroformylation activity.

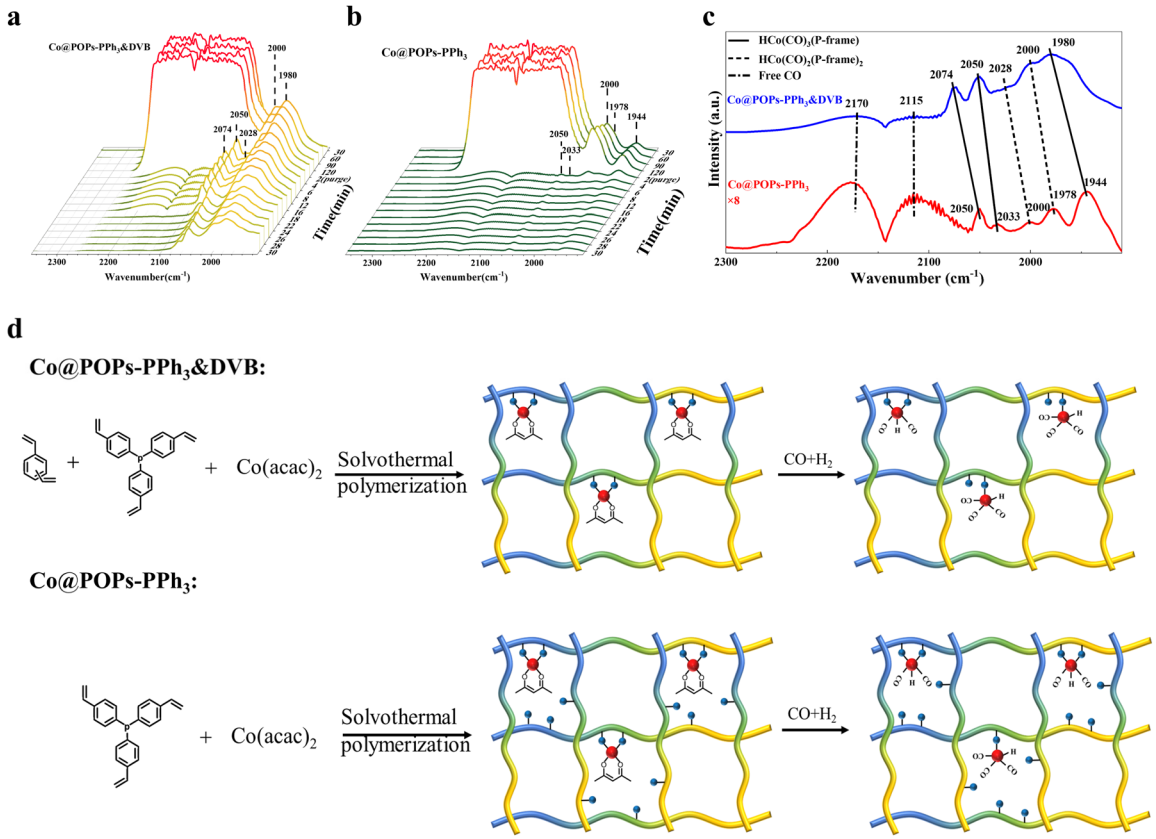

Fig. 5 (a) *In situ* DRIFTs of Co@POPs-PPh_3&DVB, the spectrum was collected after syngas adsorption (120 min) and N_2 purging (30 min); (b) *in situ* DRIFTs of Co@POPs-PPh_3, the spectrum was collected after syngas adsorption (120 min) and N_2 purging (30 min); (c) infrared spectrum comparison of Co@POPs-PPh_3&DVB and Co@POPs-PPh_3, N_2 purging (2 minutes). Note: in the Co@POPs-PPh_3&DVB sample, the molar ratio of 3v-PPh_3 to DVB is 3 : 10; and (d) solvothermal polymerization and activation process of Co@POPs-PPh_3&DVB and Co@POPs-PPh_3. Note: in the Co@POPs-PPh_3&DVB sample, the molar ratio of 3v-PPh_3 to DVB is 3 : 10.

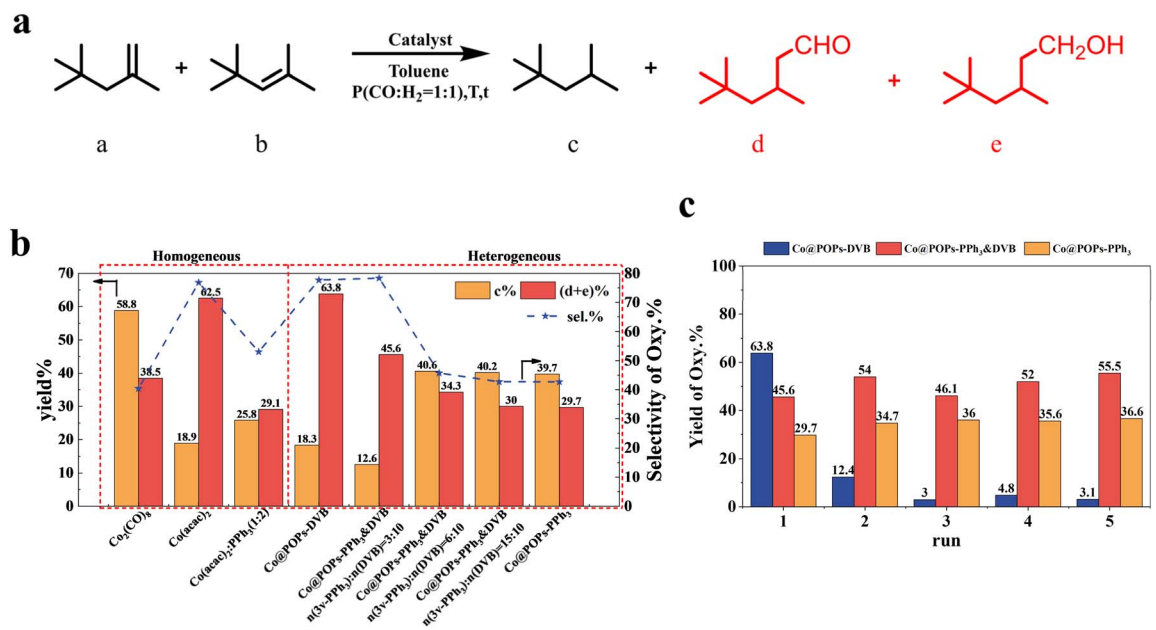

Fig. 6 (a) Chemical reaction formula for diisobutylene; (b) comparison of catalytic performance of diisobutylene hydroformylation; (c) recyclability tests of Co@POPs-DVB, Co@POPs-PPh_3&DVB, and Co@POPs-PPh_3. Note: in the Co@POPs-PPh_3&DVB sample, the molar ratio of 3v-PPh_3 to DVB is 3 : 10.

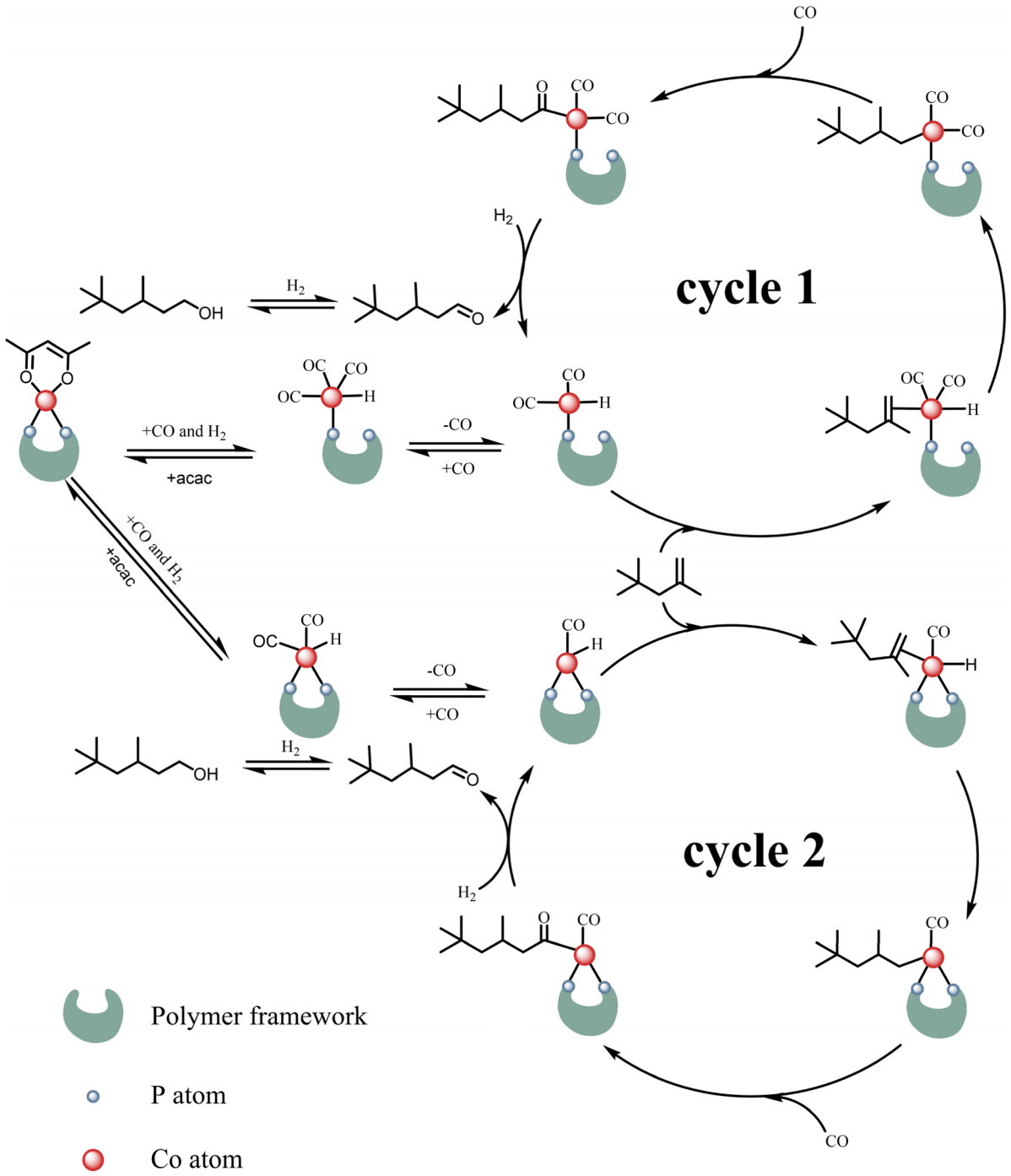

Scheme 1 Proposed mechanism of Co@POPs.

4. Conclusion

In conclusion, a series of catalysts, Co@POPs-DVB, Co@POPs-PPh_3&DVB, and Co@POPs-PPh_3, with a tunable coordination microenvironment of Co sites embedded in the POPs skeleton, were successfully designed and synthesized for the hydroformylation of diisobutylene. Among them, Co@POPs-PPh_3&DVB showed superior catalytic performance, with the yield and selectivity of oxygenated compounds as high as 45.6% and 78.4%, respectively, and a continuous reuse for 5 times without activity loss. Various characterization techniques demonstrated that the microenvironment of the single-Co-site (Co@POPs-PPh_3&DVB) was effectively tuned. The DVB building blocks increased the rigidity and reduced the pore size of the polymer, ensuring that Co@POPs-PPh_3&DVB possessed relatively lower P occupancy in the syngas atmosphere. Therefore, compared with the Co@POPs-PPh_3 catalyst constructed only by 3v-PPh_3 blocks, Co@POPs-PPh_3&DVB was more likely to form the $HCo(CO)_3$(P-

frame) active species, which possessed higher selectivity for oxygenates in the hydroformylation of diisobutylene. This work deepened our understanding of Co@POPs catalysts, demonstrating the potential industrial application perspective in hydroformylation reactions.

Conflicts of interest

There are no conflicts to declare.

Data availability

Supplementary information is available. See DOI: **https://doi.org/10.1039/d5ta04135j**.

Acknowledgements

This work was supported by the National Key R&D Program of China (No. 2023YFA1507500,2023YFA1508003), the National Natural Science Foundation of China (No. 22002152, 22108275), the Strategic Priority Research Program of the Chinese Academy of Sciences (No. XDA 21020900, XDA29050300), Youth Innovation Promotion Association CAS (No. 2023190, 2021181), the Natural Science Foundation of Liaoning Province-Outstanding Youth Science Foundation (No. 2024JH3/10200014), the Dalian Outstanding Young Scientific and Technological Talents (No. 2024RY016), and the Dalian Institute of Chemical Physics (No. DICP I202455, DICP I202134). Co K-edge X-ray absorption fine structure (EXAFS and XANES) spectra were obtained at the BL14W1 beamline of Shanghai Synchrotron Radiation Facility (SSRF) and the Shanghai Institute of Applied Physics (SINAP), Chinese Academy of Sciences. Technical support and helpful discussion by Dr Fanfei Sun are gratefully acknowledged. Dalian Institute of Chemical Physics, the HAADF-STEM support by Dr Yang Zhao is gratefully acknowledged. Dalian National Laboratory for Clean Energy, Dalian Institute of Chemical Physics, Chinese Academy of Sciences is acknowledged, and Guoqing Wang is especially thanked for his active participation in the discussion of this study.

References

1 R. Franke, D. Selent and A. Börner, *Chem. Rev.*, 2012, **112**, 5675–5732.
2 B. Zhang, D. Peña Fuentes and A. Börner, *ChemTexts*, 2021, **8**, 2.
3 S. Siangwata, N. J. Goosen and G. S. Smith, *Appl. Catal. Gen.*, 2020, **603**, 117736.
4 D. S. Ramarou, B. C. Makhubela and G. S. Smith, *Inorg. Chim. Acta*, 2019, **496**, 119051.
5 P. J. Baricelli, M. Rodriguez, L. G. Melean, M. Borusiak, I. Crespo, J. C. Pereira and M. Rosales, *Mol. Catal.*, 2020, **497**, 111189.
6 F. G. Delolo, J. Yang, H. Neumann, E. N. dos Santos, E. V. Gusevskaya and M. Beller, *ACS Sustain. Chem. Eng.*, 2021, **9**, 5148–5154.
7 D. M. Hood, R. A. Johnson, A. E. Carpenter, J. M. Younker, D. J. Vinyard and G. G. Stanley, *Science*, 2020, **367**, 542–548.
8 F. G. Delolo, C. Kubis, B. Zhang, H. Neumann, E. N. dos Santos, E. V. Gusevskaya and M. Beller, *Catal. Sci. Technol.*, 2024, **14**, 1524–1533.
9 G. Achonduh, Q. Yang and H. Alper, *Tetrahedron*, 2015, **71**, 1241–1246.
10 H.-W. Bohnen and B. Cornils, *Adv. Synth. Catal.*, 2002, **47**, 1–64.
11 H. Wang, H. Yuan, X. Chen, X. Wang, K. Zhao and F. Shi, *J. Phys. Chem. C*, 2021, **126**, 273–281.
12 D. He, D. Pang, T.-e. Wang, Y. Chen, Y. Liu, J. Liu and Q. Zhu, *J. Mol. Catal. A: Chem.*, 2001, **174**, 21–28.
13 X. Zhao, K. Guo, Y. Song, Q. Shi and Y. Xu, *Chem. Ind. Eng. Prog.*, 1999, **18**, 23–26.
14 M. F. Hertrich, F. K. Scharnagl, A. Pews-Davtyan, C. R. Kreyenschulte, H. Lund, S. Bartling, R. Jackstell and M. Beller, *Chem.–Eur. J.*, 2019, **25**, 5534–5538.
15 J. Zhao, Y. He, F. Wang, W. Zheng, C. Huo, X. Liu, H. Jiao, Y. Yang, Y. Li and X. Wen, *ACS Catal.*, 2019, **10**, 914–920.
16 B. Wei, X. Liu, Y. Deng, K. Hua, J. Chen, H. Wang and Y. Sun, *ACS Catal.*, 2021, **11**, 14319–14327.
17 J. Zhao, Y. He, F. Wang, Y. Yang, W. Zheng, C. Huo, H. Jiao, Y. Yang, Y. Li and X. Wen, *J. Catal.*, 2021, **404**, 244–249.
18 S. Zhang, J. Chen, B. Wei, H. Zhou, K. Hua, X. Liu, H. Wang and Y. Sun, *J. Am. Chem. Soc.*, 2024, **146**, 6037–6044.
19 H. Gong, X. Zhao, Y. Qin, W. Xu, X. Wei, Q. Peng, Y. Ma, S. Dai, P. An and Z. Hou, *J. Catal.*, 2022, **408**, 245–260.
20 X. Wang, C. Wang, H.-Q. Tan, T.-Y. Qiu, Y.-M. Xing, Q.-K. Shang, Y.-N. Zhao, X.-Y. Zhao and Y.-G. Li, *Chem. Eng. J.*, 2022, **431**, 134051.
21 G. Wang, M. Jiang, G. Ji, Z. Sun, L. Ma, C. Li, H. Du, L. Yan and Y. Ding, *Catalysts*, 2021, **11**, 220.
22 R. Das, R. Kishan, D. Muthukumar, R. S. Pillai and C. Nagaraja, *J. Environ. Chem. Eng.*, 2024, **12**, 113777.
23 S. Feng, M. Jiang, X. Song, P. Qiao, L. Yan, Y. Cai, B. Li, C. Li, l. Ning and S. Liu, *Angew. Chem., Int. Ed.*, 2023, **62**, 202304282.
24 C. Li, L. Yan, L. Lu, K. Xiong, W. Wang, M. Jiang, J. Liu, X. Song, Z. Zhan and Z. Jiang, *Green Chem.*, 2016, **18**, 2995–3005.
25 M. Jiang, L. Yan, Y. Ding, Q. Sun, J. Liu, H. Zhu, R. Lin, F. Xiao, Z. Jiang and J. Liu, *J. Mol. Catal. A: Chem.*, 2015, **404**, 211–217.
26 G. Wang, M. Jiang, Z. Sun, L. Qian, G. Ji, L. Ma, C. Li, Z. Wang, Y. Yang and X. Lin, *Chem. Eng. J.*, 2023, **476**, 146332.
27 K. Zhao, H. Wang, X. Wang, T. Li, X. Dai, L. Zhang, X. Cui and F. Shi, *J. Catal.*, 2021, **401**, 321–330.
28 G. Ji, C. Li, X. Lin, X.-F. Wu, L. Yan and Y. Ding, *ACS Sustain. Chem. Eng.*, 2022, **10**, 15467–15479.
29 G. Ji, C. Li, D. Xiao, G. Wang, Z. Sun, M. Jiang, G. Hou, L. Yan and Y. Ding, *J. Mater. Chem. A*, 2021, **9**, 9165–9174.
30 Y. Wang, M. Jiang, L. Yan, C. Li, G. Wang, W. He and Y. Ding, *Mol. Catal.*, 2023, **539**, 113015.
31 B. Fan, M. Jiang, G. Wang, Y. Zhao, B. Mei, J. Han, L. Ma, C. Li, G. Hou and T. Wu, *Nat. Commun.*, 2024, **15**, 6967.

32 F. J. Escobar-Bedia, M. Lopez-Haro, J. J. Calvino, V. Martin-Diaconescu, L. Simonelli, V. Perez-Dieste, M. J. Sabater, P. Concepción and A. Corma, *ACS Catal.*, 2022, **12**, 4182–4193.
33 B. Wei, X. Liu, Q. Chang, S. Li, H. Luo, K. Hua, S. Zhang, J. Chen, Z. Shao, C. Huang, H. Wang and Y. Sun, *Chem Catal.*, 2022, **2**, 2066–2076.
34 S. Kinoshita, F. Shibahara and K. Nozaki, *Green Chem.*, 2005, **7**, 256–258.
35 W. Jiang, J. Li, M. Wu, L. He, G. Zhou and Z. Wang, *Fuel*, 2023, **338**, 127291.
36 Y. Li, Z. Zhao, W. Lu, M. Jiang, C. Li, M. Zhao, L. Gong, S. Wang, L. Guo and Y. Lyu, *ACS Catal.*, 2021, **11**, 14791–14802.
37 Q. Sun, M. Jiang, Z. Shen, Y. Jin, S. Pan, L. Wang, X. Meng, W. Chen, Y. Ding and J. Li, *Chem. Commun.*, 2014, **50**, 11844–11847.
38 J. Perera, D. Frost and C. McDowell, *J. Chem. Phys.*, 1980, **72**, 5151–5158.
39 J. Sun, G. Yu, L. Liu, Z. Li, Q. Kan, Q. Huo and J. Guan, *Catal. Sci. Technol.*, 2014, **4**, 1246–1252.
40 M. Pelavin, D. Hendrickson, J. Hollander and W. Jolly, *J. Phys. Chem. C*, 1970, **74**, 1116–1121.
41 D. M. Hood, R. A. Johnson, D. J. Vinyard, F. R. Fronczek and G. G. Stanley, *J. Am. Chem. Soc.*, 2023, **145**, 19715–19726.
42 M. Van Boven, N. Alemdaroglu and J. Penninger, *Ind. Eng. Chem. Res.*, 1975, **14**, 259–264.
43 M. Van Boven, N. Alemdaroğlu and J. Penninger, *J. Organomet. Chem.*, 1975, **84**, 65–74.
44 A. Misono, Y. Uchida, M. Hidai and T. Kuse, *Chem. Commun.*, 1968, **16**, 981.